Available online at www.sciencedirect.com
SCIENCE DIRECT®

Physics of the Earth and Planetary Interiors 155 (2006) 63–72

PHYSICS OF THE EARTH AND PLANETARY INTERIORS

www.elsevier.com/locate/pepi

Spatially dependent seismic anisotropy in the Tonga subduction zone: A possible contributor to the complexity of deep earthquakes

Václav Vavryčuk *

Geophysical Institute, Academy of Sciences of the Czech Republic, Boční II/1401, 141 31 Praha 4, Czech Republic

Received 17 December 2004; received in revised form 4 August 2005; accepted 7 October 2005

Abstract

The deep part of the Tonga subduction zone consists of two differently oriented slab segments: the northern segment within latitudes 17–19°S, and the southern segment within latitudes 19.5–27°S. The orientation of the slab is (strike/dip): 110°/57° in its northern part and 210°/46° in its southern part. Both segments are seismically active at depths from 500 to 700 km. The mechanisms of deep-focus earthquakes reported in the Harvard moment tensor catalogue contain compensated linear vector dipole (CLVD) components that behave differently in both segments. The mean value of the CLVD is 3% for the northern segment but −10% for the southern segment. The mean absolute value of the CLVD is 12% for the northern segment and 16% for the southern segment. The complex behaviour of the CLVD is explained by spatially dependent seismic anisotropy in the slab. The inversion for anisotropy from the non-double-couple components of moment tensors points to orthorhombic anisotropy in the both slab segments. The anisotropy seems to have a uniform strength of 5–7% for *P*-waves and 9–12% for *S*-waves, and is oriented according to the orientation of each segment and the stress acting in it. The spatial variation of velocities is roughly similar in both segments. The retrieved anisotropy might have several possible origins. It can be: (1) intrinsic, caused by preferentially aligned anisotropic minerals such as wadsleyite, ringwoodite, ilmenite or others, (2) effective, caused, for example, by intra-slab layering, or (3) partly apparent, produced by systematic errors in the moment tensors due to neglecting 3D slab geometry and the slab/mantle velocity contrast when calculating the Green functions in the moment tensor inversion.

Keywords: Deep-focus earthquakes; Earthquake mechanism; Seismic anisotropy; Subduction zones

1. Introduction

Since subducting slabs are exposed to extremely high stress present in the mantle, it is assumed that rock-forming minerals in slabs, such as olivine or its polymorphs wadsleyite and ringwoodite, are aligned due to stress and produce the intra-slab seismic anisotropy. For example, olivine has orthorhombic symmetry, its *P* anisotropy is 25% and the *S* anisotropy is 18%. Wadsleyite has the same symmetry with *P* and *S* anisotropy strength of 16.9% and 17.7%, respectively (Mainprice et al., 2000). To assess the overall anisotropy in the slab is highly desirable, because it can help us to understand the behaviour of rocks under anomalous pressure and temperature conditions, and to study the structure and mineralogical composition of the slab and their changes owing to the 220, 410 and 520 km discontinuities.

So far anisotropy of slabs and of the surrounding mantle has been studied mainly using the splitting of *S*-, *SKS*-, *ScS*-, or *sScS*-waves (Babuška and Cara, 1991;

* Fax: +420 272761549.
E-mail address: vv@ig.cas.cz.

0031-9201/$ – see front matter © 2005 Elsevier B.V. All rights reserved.
doi:10.1016/j.pepi.2005.10.005

Savage, 1999). The studies suggest anisotropy in various slabs of up to 5% (Fukao, 1984; Hiramatsu and Ando, 1996; Hiramatsu et al., 1997; Fouch and Fischer, 1996, 1998; Wookey et al., 2002). However, these values are uncertain, because the method measures the overall anisotropy along a whole ray path and cannot segregate anisotropy of a slab from that of the surrounding mantle. Recently, Vavryčuk (2004) proposed an inversion for anisotropy, which overcomes the mentioned difficulty. The method uses non-double-couple (non-DC) components of moment tensors of earthquakes and yields a local anisotropy just in the focal area. This method is, in particular, proper for studying anisotropy in slabs, because it can exploit deep-focus earthquakes. Since the method requires a large number of highly accurate moment tensors, a suitable area for its application is the Tonga subducting slab that is associated with the most intense deep seismicity in the world.

The Tonga subduction zone is the result of the Pacific Plate subducting under the Australian Plate. The Pacific plate moves at a rate of 10.5 cm/year (DeMets et al., 1990; Gripp and Gordon, 1990). The direction of motion is N300°E, being perpendicular to the strike of the slab and the Tonga-Kermadec Trench. The slab subducts steeply with a dip of about 60°. However, this value can vary with depth (Northard et al., 1996). At depths greater than 500 km, the geometry of the slab is complicated. The slab is deformed and sharply bent in the northern part of the slab. This causes the strikes of the northern and southern parts of the slab to be remarkably different (Giardini and Woodhouse, 1984; Hamburger and Isacks, 1987; Giardini, 1992).

In this paper, I shall extend the work by Vavryčuk (2004), where anisotropy of just one segment of the Tonga slab has been studied. Here, I shall study and compare two different slab segments. I shall show that the complexity in the geometry of the Tonga slab projects partly into the complex behaviour of the non-DC mechanisms of deep-focus earthquakes in the slab. Using the moment tensors of the earthquakes that occurred in the different segments of the slab, I shall invert for a possible anisotropy in the slab and try to map its spatial variation.

2. Deep earthquakes in the Tonga subduction zone

2.1. Data

I use moment tensors of earthquakes available in the Harvard centroid moment tensor (CMT) catalogue (Dziewonski et al., 1981, 2001, 2003; Dziewonski and Woodhouse, 1983). This global earthquake catalogue

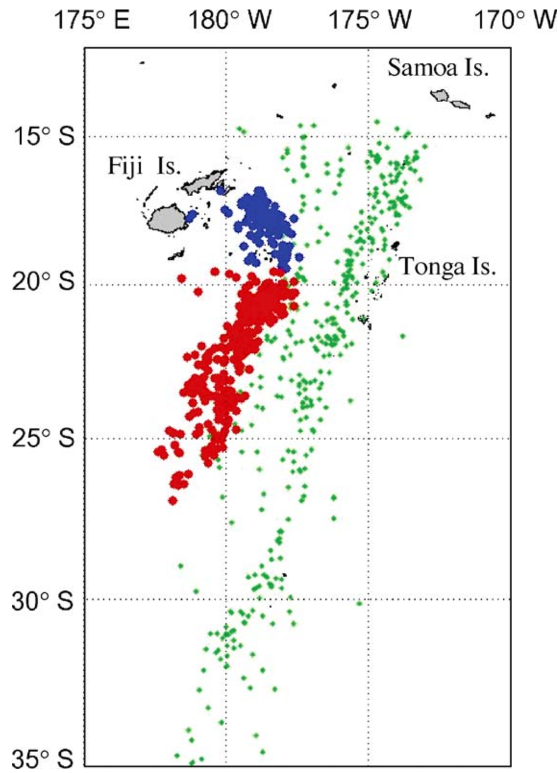

Fig. 1. Epicentres of earthquakes in the Tonga subduction zone. Green dots mark earthquake foci at depths between 100 and 500 km, blue/red dots mark deep-focus earthquakes at depths greater than 500 km in the northern/southern cluster.

seems best in completeness and reports also the accuracy of its solutions (Frohlich and Davis, 1999; Helffrich, 1997; Kagan, 2003). I have selected earthquakes with magnitudes $M_W > 5$, which occurred in the period 1980–2003, and were located at latitudes 17–27°S, longitudes 178–183°E and at depths ranging from 500 to 700 km. These earthquakes were sorted into two families: 157 earthquakes with foci at latitudes 17–19°S (Fig. 1, blue dots) and 387 earthquakes with foci at latitudes 19.5–27°S (Fig. 1, red dots). The two families of earthquakes were selected to occur in differently oriented northern and southern parts of the slab. The earthquakes within latitudes 19.0–19.5°S were discarded, because they belong to a highly deformed transition zone between both the slab segments.

The selected moment tensors were decomposed into the double-couple (DC) and non-double-couple (non-DC) components according to Eqs. (10)–(17) of Vavryčuk (2005). The moment tensors are of different accuracy and display a different amount of non-DC components. The non-DC components contain only the compensated linear vector dipole (CLVD) component. The isotropic (ISO) component is identically zero, because of constraints imposed on the CMT inversion. In order to analyze the most reliable moment tensors, only moment tensors with the absolute value of the CLVD less than 40% were considered. The moment tensors with the CLVD higher than 40% were discarded because they indicate either an anomalous mechanism or difficulties in the moment tensor inversion. Furthermore, only moment tensors with relative error e less than 0.08 were analyzed. The relative error e is defined as the ratio of the largest singular values of standard error $\mathbf{E}$ reported in the catalogue and of moment tensor $\mathbf{M}$. The value $e = 0.08$ was found to be an optimum compromise between demands for a large number of moment tensors and for their high accuracy needed in the anisotropy inversion (Vavryčuk, 2004). Hence, the final datasets comprised moment tensors of 41 and 88 for the northern and southern parts of the slab, respectively.

2.2. Foci clustering, focal mechanisms and stress in the slab

Interpolating foci of the selected earthquakes by a plane, we can infer the orientation of the slab segments. The results are summarized in Table 1. The errors of the strike and dip are about 5° and 10°, respectively. The strike of the southern part of the slab at depths 500–700 km correlates well with the strike of the slab at other depths and corresponds to the strike of the Tonga-Kermadec Trench. However, this part of the slab is slightly steeper at shallower depths (the dip increases to 60°). The strike of the northern part of the slab is anomalous and points to a complex deformation of the slab at depths 500–700 km.

The focal mechanisms in the northern part of the slab vary with no preferential type of faulting (Fig. 2). The focal mechanisms in the southern part of the slab are mainly normal or reverse with subvertical and subhorizontal nodal planes (Fig. 3). In both slab segments, the P axes form a more compact cluster than the T axes, which are more scattered. This might indicate a minor difference between the σ_2 and σ_3 principal stresses. The orientation of the principal stress axes for each segment of the slab was determined from focal mechanisms by applying the inversion method of Gephart and Forsyth (1984). The inversion was performed using a 5° grid in searching through the principal stress directions and a 0.02 increment in searching for σ_2 (assuming $\sigma_1 = -1$ and $\sigma_1 + \sigma_2 + \sigma_3 = 0$). The misfit function is shown in Fig. 4. The optimum stress directions are summarized in Table 1.

The best constrained stress axis in both segments of the slab is the axis for the maximum compression σ_1. The maximum compression in the southern slab segment follows the subduction flow; the other stress axes lie in the slab and along the normal to the slab. The down-dip compression in the deep part of a slab is observed frequently (Isacks and Molnar, 1971; Frohlich, 1989; Guest et al., 2004) and interpreted as resistance to subduction due to resisting forces at the tip of the slab (Zhou, 1990). The stress axes in the northern slab segment are only slightly rotated (clockwise by 20–30°) with respect to the southern segment, but the principal stresses are interchanged (see Fig. 4). Two stress directions lie again in the slab segment and the third axis is close to its normal.

2.3. Non-DC components in moment tensors and their origin

Deep earthquakes often display non-DC components (Frohlich, 1989; Julian et al., 1998; Kuge and Kawakatsu, 1992). The non-DC components contain mainly the CLVD; the ISO is reported to be zero or very small (not exceeding 10%, Kawakatsu, 1991, 1996). Therefore, the non-DC components cannot be produced primarily by phase transitions, because the phase transitions are accompanied with volume changes and should generate a significant ISO component. The non-DC components in the selected moment tensors probably have three major origins: First, part of them is spurious being produced by inaccurate moment tensor inversion. The inaccuracies can originate from an oversimplified Earth's velocity model used for calculating the Green functions (Šílený and Vavryčuk, 2000, 2002) and from the limited number of data inverted. For example, the slab itself

Table 1
Slab orientation and stress in the slab

Dataset	Moment tensors	Relative error (%)	Slab strike/dip (°)	Slab normal az/dip (°)	Sigma 1 az/dip (°)	Sigma 2 az/dip (°)	Sigma 3 az/dip (°)
Northern cluster	41	0.08	110/57	20/57	250/65	355/55	130/45
Southern cluster	88	0.08	210/46	120/46	320/45	140/45	230/90

The azimuth is measured from the north and the dip from the vertical.

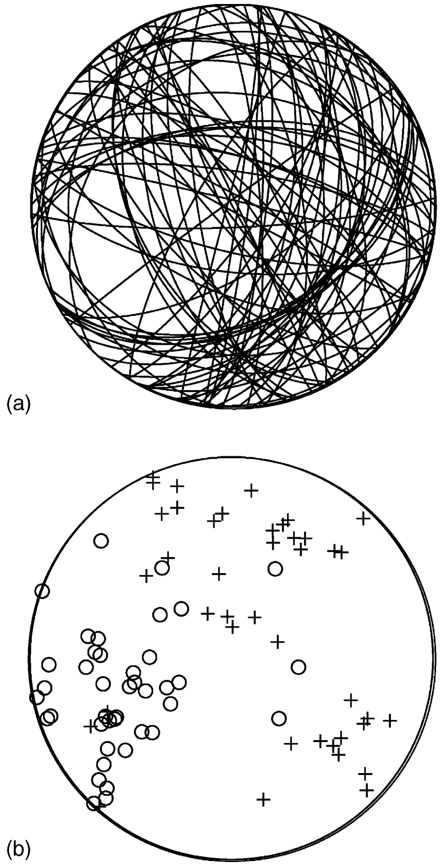

Fig. 2. Nodal lines (a) and *P*–*T* axes (b) for the 41 earthquakes located in the northern cluster. The *P* axes are marked by circles, the *T* axes are marked by plus signs.

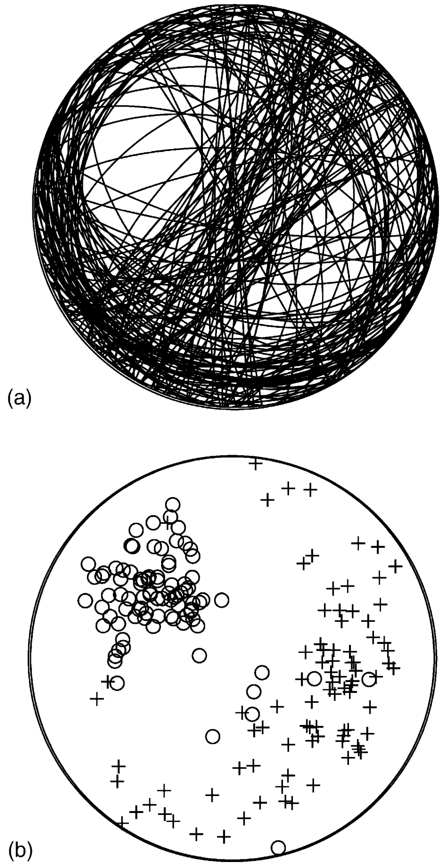

Fig. 3. Nodal lines (a) and *P*–*T* axes (b) for the 88 earthquakes located in the southern cluster. The *P* axes are marked by circles, the *T* axes are marked by plus signs.

is a high-velocity inhomogeneity which is not taken into account in the global Earth's velocity model. The effects of 3D slab structure on amplitudes (see Kendall and Thomson, 1993) can thus introduce artefacts in the standard moment tensor inversions. Second, the non-DC components can be generated by complex shear faulting at non-planar faults (Miller et al., 1998; Tibi et al., 2003). This type of faulting generates no ISO component, which is in coincidence with observations. Third, the non-DC components can be produced by anisotropy in the slab (Kawasaki and Tanimoto, 1981; Frohlich, 1994). Anisotropy at the source area can also generate non-DC mechanisms with no or very small ISO component (see Vavryčuk, 2004, 2005). Obviously, all three mentioned origins can produce non-DC mechanisms separately, but it is very like that they combine and that the non-DC components contain contributions of all of them. The part of the non-DC components which is spurious can be reduced by selecting only very accurate moment tensors. However, the other parts of the non-DC components are mixed and cannot be easily separated.

The accuracy of the CLVD (and the presence of the spurious non-DC) can be roughly assessed by correlating the CLVD of the earthquakes reported jointly in the CMT and USGS (Sipkin et al., 2002) catalogues. Surprisingly, this correlation differs for both clusters (see Table 2): the northern cluster comprises 22 jointly reported moment tensors with a correlation of 0.74, while the southern cluster comprises 53 jointly reported moment tensors with a correlation of 0.57. The mentioned datasets comprise earthquakes with the relative error *e* of the CMT moment tensors less than 0.08 and with no constraint on the CLVD. The evident positive correlation demonstrates that the major part of the CLVD is not spurious, but must have a physical origin. The lower correlation of the CLVD for the southern cluster indicates that the CLVD in this cluster is determined with a slightly lower accuracy than for the northern cluster. This might be caused by less favourable station

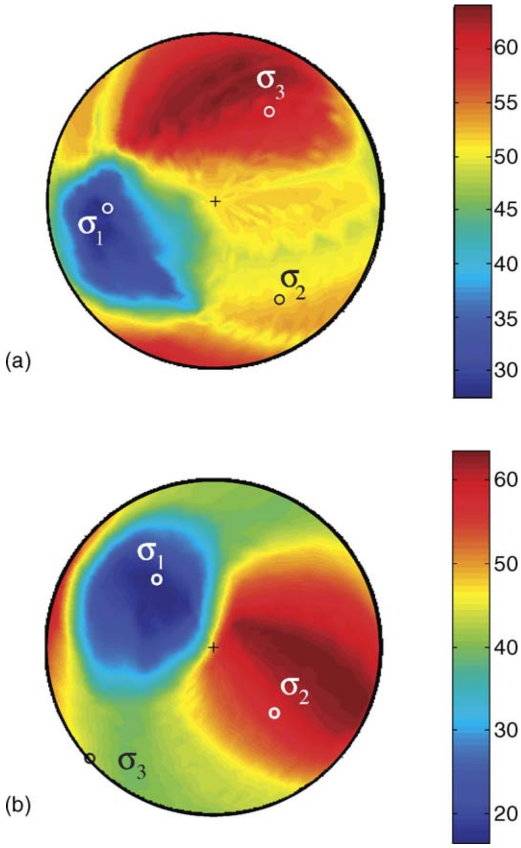

Fig. 4. Inversion for stress in the northern (a) and southern (b) slab segments. The plot shows the misfit function for the stress axis σ_1, defined as an average deviation (in degrees) between predicted shear traction directions and observed slips at the faults. The misfit functions are displayed in the lower-hemisphere equal-area projection. The optimum directions of the principal stresses are marked by circles.

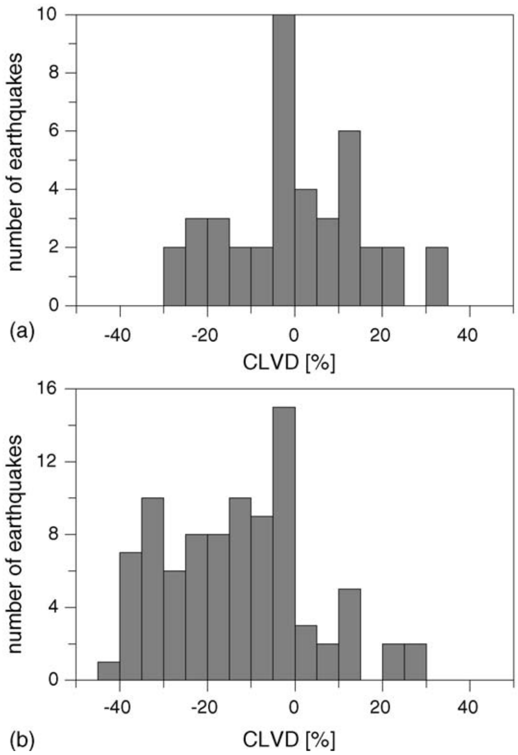

Fig. 5. Histograms of the CLVD percentages in the moment tensors of the northern (a) and southern (b) clusters. The ISO components are identically zero, because the moment tensors are constrained to have zero trace.

coverage used in the moment tensor inversion for this area.

Not only the accuracy, but also the percentage of the CLVD differs in both the studied datasets. In the northern cluster, the CLVD attains equally positive and negative values and the average CLVD is close to zero (see Table 2; Fig. 5). In the southern cluster, the CLVD is mostly negative. The average absolute value of the CLVD is higher for the southern cluster. This indicates that the moment tensors in this cluster are on average more non-DC than those in the northern cluster.

The different behaviour of non-DC components in both datasets of moment tensors is an intriguing phenomenon. It cannot be produced by errors in the moment tensor inversion, because only the most reliable moment tensors were considered. Moreover, the differences in the average trend of the non-DC components tend to increase with increasing accuracy of moment tensors (by decreasing the value of relative error e). Also, the differences can hardly be explained by different complexities in earthquake sources in both parts of the slab. Most probably, the differences in the CLVD indicate a different anisotropy

Table 2
Observed DC and non-DC components in moment tensors

Data set	Moment tensors	Relative error (%)	Mean DC (%)	Mean CLVD (%)	Mean |CLVD| (%)	Joint moment tensors	Correlation CLVD
Northern cluster	41	0.08	88.1	2.9	11.9	22	0.74
Southern cluster	88	0.08	84.3	−10.6	15.7	53	0.57

The DC and CLVD percentages were calculated using Eqs. (8a–c) of Vavryčuk (2001).

or a different orientation of faulting with respect to the anisotropy in the slab.

3. Anisotropy of the subduction zone

The fact that the non-DC components detected in moment tensors are not produced only by anisotropy, but also have other origins, makes the inversion for anisotropy particularly difficult. Nevertheless, even though the non-DC components are remarkably affected by causes other than anisotropy, Vavryčuk (2004) showed on synthetic tests that if a sufficiently large dataset of moment tensors with non-DC components is collected, the inversion can produce reasonable estimates of anisotropy.

3.1. Principles of the inversion

The seismic moment tensor **M** of a shear earthquake in anisotropic media is expressed as (Vavryčuk, 2005, Eq. (4)):

$$M_{ij} = c_{ijkl} D_{kl}, \tag{1}$$

where c_{ijkl} are the elastic parameters of the medium, and D_{kl} is the source tensor defined as

$$D_{kl} = \frac{uS}{2}(\nu_k n_l + \nu_l n_k). \tag{2}$$

Vectors $\boldsymbol{\nu}$ and **n** specify the fault normal and slip direction, u is the slip and S is the fault area. The source tensor **D** depends just on geometry of faulting and it should satisfy the following two conditions:

$$\mathrm{Trace}(\mathbf{D}) = 0, \tag{3}$$

$$\mathrm{Det}(\mathbf{D}) = 0. \tag{4}$$

The first equation is the condition for shear faulting, and the second equation follows from the fact that tensor **D** has one zero eigenvalue. Both equations can be advantageously used in defining the misfit function in the inversion for anisotropy. If we know moment tensors of many earthquakes that occurred at the same source area, we can invert for elastic parameters c_{ijkl} minimizing the sum of absolute values of Trace(**D**) and Det(**D**) for all earthquakes. The method can be modified to be applicable also for the inversion from moment tensors, which are constrained to have zero trace (see Vavryčuk, 2004). As expected, if we invert DC moment tensors, the procedure yields isotropic medium; if we invert the non-DC mechanisms, we obtain anisotropy.

3.2. Inversion for orthorhombic anisotropy

The quality and extent of the data makes it possible to invert for orthorhombic or monoclinic anisotropy. The orthorhombic anisotropy is typical for mantle minerals such as olivine, wadsleyite, or ringwoodite (Mainprice et al., 2000). Since the inversion for monoclinic anisotropy yields essentially the same results as for orthorhombic anisotropy, but the inversion is less stable (because three more parameters are sought), only the results for orthorhombic anisotropy are presented. The inversion for triclinic anisotropy was not feasible because of limitations of data.

The inversion seeks to determine three angles θ, φ and ψ defining the directions of the symmetry axes, and nine density-normalized elastic parameters (in the Voigt notation) A_{11}, A_{22}, A_{33}, A_{44}, A_{55}, A_{66}, A_{12}, A_{13}

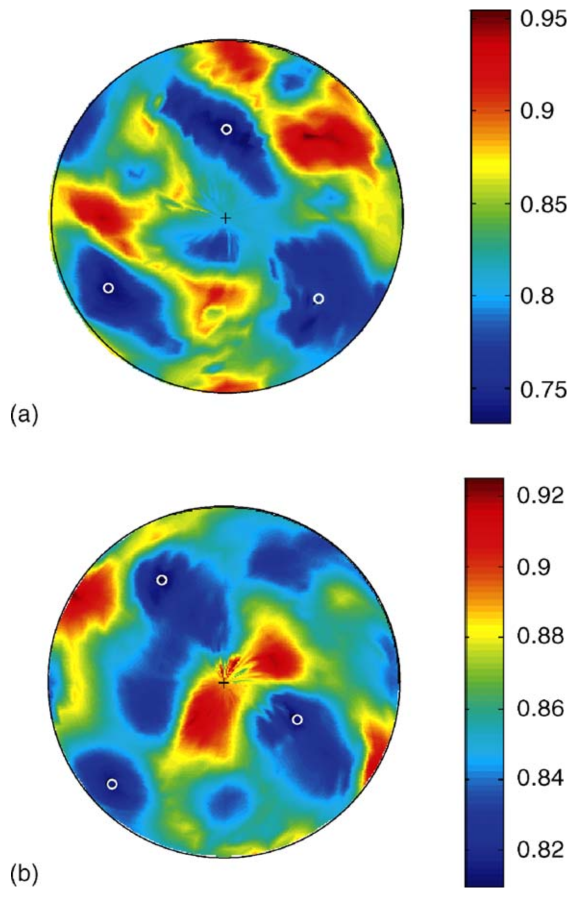

Fig. 6. Inversion for orthorhombic anisotropy in the northern (a) and southern (b) slab segments. The plot shows the misfit functions for symmetry axes of orthorhombic anisotropy, normalized to the misfit for an isotropic medium. The misfit functions are displayed in the lower-hemisphere equal-area projection. The optimum directions of the symmetry axes of anisotropy are marked by circles.

Table 3
Orientation and strength of anisotropy

Dataset	Axis 1 az/dip (°)	Axis 2 az/dip (°)	Axis 3 az/dip (°)	*P*-wave anisotropy (%)	*S*1-wave anisotropy (%)	*S*2-wave anisotropy (%)
Northern cluster	360/40	135/60	240/65	4.8 ± 0.4	10.7 ± 1.0	9.4 ± 1.1
Southern cluster	330/60	115/35	230/75	6.5 ± 1.2	10.2 ± 2.0	11.9 ± 0.9

The anisotropy strength is calculated as the median from strengths of 25 best anisotropy models, and the errors are defined as the standard deviations.

and A_{23}, defining orthorhombic anisotropy. The angles of the symmetry axes varied in a grid with a step of 5°. For each direction of the symmetry axes, a constrained non-linear optimization search for optimum values of elastic parameters was applied (Branch and Grace, 1996), and the misfit function was evaluated. The inversion for the optimum elastic parameters was constrained to fix the squares of the spatially averaged *P* and *S* velocities estimated from the isotropic Earth's velocity model AK135 (Kennett et al., 1995). The starting values of the sought parameters, inversion limits and other details of the inversion algorithm are in Vavryčuk (2004).

3.3. Orientation and strength of anisotropy

The results of the inversions are summarized in Table 3. Fig. 6 shows the misfit functions evaluated for each direction of the symmetry axis a_3 of orthorhombic anisotropy when inverting moment tensors of the northern and southern clusters. The misfit function is normalized so that it equals 1 for an isotropic medium. The function displays only three distinct minima. The directions of the minima are mutually perpendicular and correspond to optimum directions of the symmetry axes. The errors in the optimum directions are about 10°. The best solutions lower the misfit function from 1 to 0.73 for the northern cluster and to 0.81 for the southern cluster; hence anisotropy is responsible only for a part of the non-DC components in moment tensors. For both clusters, two symmetry axes lie within the slab, the third axis is close to the direction of the normal to the slab. The directions of the symmetry axes coincide with the directions of the principal stress axes (see Fig. 7). The anisotropy strength is similar for both clusters. The *S* anisotropy is almost twice stronger than the *P* anisotropy. In spite of similarities, the detailed spatial variation of velocities in both slab segments is slightly different (see Fig. 8). This might be caused by different stress conditions in both slab segments.

3.4. Predicted non-DC components in the slab

From the retrieved optimum anisotropy we can predict non-DC components generated in the moment tensors (Table 4). The ISO component is significantly smaller than the CLVD for both slab segments. The small predicted values of the ISO could explain why the ISO components have not been detected reliably so far (Kawakatsu, 1991, 1996; Hara et al., 1995). The correlation between the observed and predicted CLVD is significant, but still points to the fact that anisotropy can-

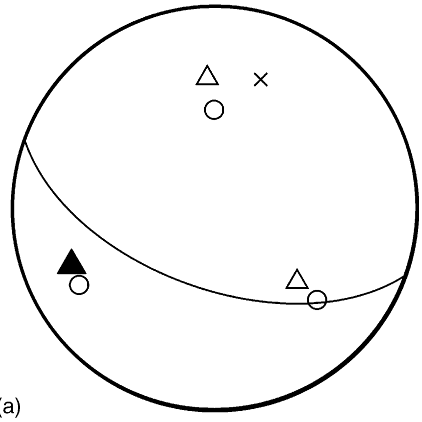
(a)

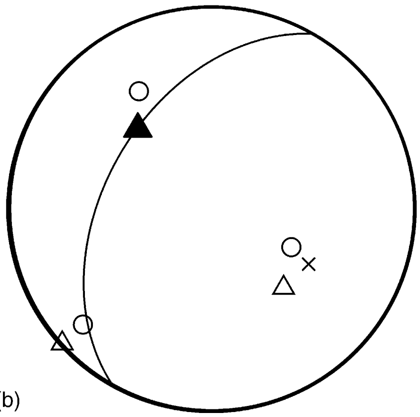
(b)

Fig. 7. A comparison of slab, stress and anisotropy orientations for the northern (a) and southern (b) slab segments. The directions of the slab normal (cross), of the principal stress axes (triangles), and of the symmetry axes of anisotropy (circles) are shown in the lower-hemisphere equal-area projection. The solid line shows the intersection of the slab with the hemisphere. The solid triangle marks the direction of the maximum compression.

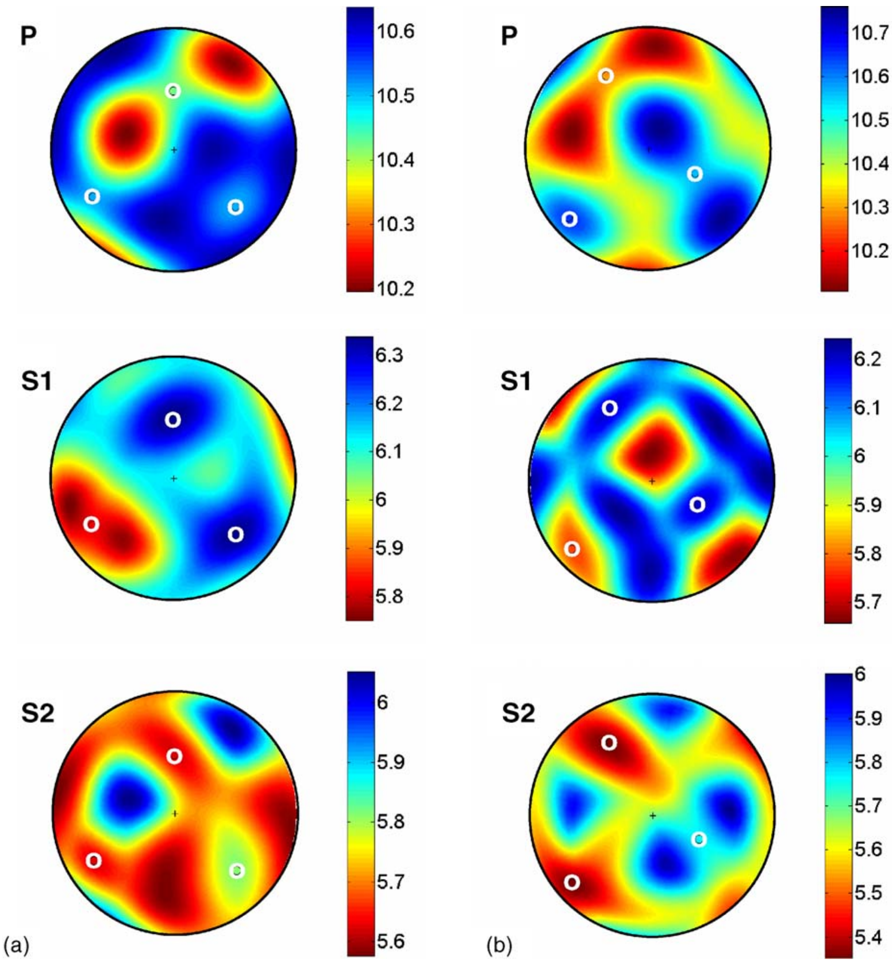

Fig. 8. Spatial variation of the P, $S1$ and $S2$ velocities predicted by the optimum anisotropy models for the northern (a) and southern (b) slab segments. Lower-hemisphere equal-area projection is used. Directions of the symmetry axes are marked by circles. Velocities are in km/s.

not fully explain the observed CLVD. Interestingly, the data in the northern slab segment are more consistent: the fit for the optimum anisotropy is better and also the correlation between the observed and predicted CLVD is better. This is perfectly consistent with the fact that the observed CLVD is more reliable for the northern rather than for the southern slab segment as was indicated by correlating the CLVD for jointly reported earthquakes in the USGS and CMT catalogues (see Table 2).

4. Summary

- The deep part of the Tonga subduction zone has a complicated geometry. The slab is sharply bent and divides into two segments with quite different strikes. The northern segment is smaller and produces fewer earthquakes than the southern segment.
- Both parts of the Tonga slab are characterized by the down-dip compression. The P axes of mechanisms

Table 4
Predicted DC and non-DC components in moment tensors

Data set	Moment tensors	Relative error (%)	Mean DC (%)	Mean ISO (%)	Mean CLVD (%)	Mean |CLVD| (%)	Correlation CLVD
Northern cluster	41	0.08	90.3	−2.0	3.7	6.6	0.57
Southern cluster	88	0.08	88.3	1.5	−8.3	10.1	0.32

Correlation CLVD means the correlation between observed and predicted values of the CLVD.

are well clustered, the T axes are rather scattered. The scatter of the T axes points to a small difference between the σ_2 and σ_3 principal stresses.

- The CLVD components in the moment tensors of deep earthquakes behave differently in both parts of the slab. The mean value of the CLVD is 3% for the northern part of the slab and −10% for the southern part of the slab. This difference must have a physical origin and is most likely caused by differently oriented anisotropy in the slab.
- Anisotropy in the slab might be one of the sources of non-DC components in deep earthquakes. So far its significance has been overlooked even though anisotropy with strength of 10% can produce CLVD up to 30–40% (Vavryčuk, 2005). The presence of anisotropy is supported by the fact that the inversion for anisotropy from non-DC mechanisms was successful. Moreover, anisotropy in the slab can explain a significant part of the CLVD observed in the moment tensors, and in accordance with observations, anisotropy generates very small ISO component (less than 5%).
- The results of the inversion indicate that the orientation of anisotropy in each slab segment coincides with the orientation of the stress. This points to a primary impact of stress on anisotropy formation. Emphasize that the coincidence between anisotropy and stress orientations is not an artefact of processing the same dataset of moment tensors in both the inversions. While the stress inversion utilizes the DC parts, the anisotropy inversion utilizes the non-DC parts of the moment tensors. The independence of the inversions has also been checked by numerical modelling.
- The strength of the P, $S1$ and $S2$ anisotropy is similar in both parts of the slab: it is $5 \pm 0.5\%$, $10.5 \pm 1\%$ and $9.5 \pm 1\%$ in the northern segment, and $6.5 \pm 1.5\%$, $10 \pm 2\%$ and $12 \pm 1\%$ in the southern segment, respectively. The errors are just rough estimates, because the influence of errors in the non-DC components used in the inversion cannot be easily evaluated. The errors might be produced, for example, by an oversimplification of the velocity model used to calculate the Green functions or by assuming the ISO component to be zero in the moment tensor inversion. Despite of the uncertainties in the errors, it is clear that the anisotropy values in the slab are remarkably higher than those of the anisotropy observed in the surrounding mantle and that the S-wave anisotropy is almost twice stronger than the P-wave anisotropy.
- The origin of anisotropy is, however, still questionable. Anisotropy might be partly intrinsic, caused by anisotropic minerals such as wadsleyite, ringwoodite, ilmenite or others preferentially aligned under stress in the slab, but it can also be effective, produced by preferentially oriented inhomogeneities within the slab such as intra-slab layering. We also cannot exclude that a part of anisotropy is apparent being introduced by systematic errors present in the moment tensors. The systematic errors arise by neglecting the slab/mantle velocity and density contrasts when calculating the Green functions in the moment tensor inversion.

Acknowledgments

The work was supported by the by the Grant Agency of the Academy of Sciences of the Czech Republic, Grant A3012309, and by the Grant Agency of the Czech Republic, Grant 205/02/0383.

References

Babuška, V., Cara, M., 1991. Seismic Anisotropy in the Earth. Kluwer Academic Publishers, London.

Branch, M.A., Grace, A., 1996. Matlab Optimization Toolbox. The MathWorks, Inc.

DeMets, C., Gordon, R.G., Argus, D.F., Stein, S., 1990. Current plate motions. Geophys. J. Int. 101, 425–478.

Dziewonski, A.M., Chou, T.-A., Woodhouse, J.H., 1981. Determination of earthquake source parameters from waveform data for studies of global and regional seismicity. J. Geophys. Res. 86, 2825–2852.

Dziewonski, A.M., Woodhouse, J.H., 1983. An experiment in the systematic study of global seismicity: centroid-moment tensor solutions for 201 moderate and large earthquakes of 1981. J. Geophys. Res. 88, 3247–3271.

Dziewonski, A.M., Ekström, G., Maternovskaya, N.N., 2000. Centroid moment tensor solutions for July–September. Phys. Earth Planet. Inter. 124, 9–23.

Dziewonski, A.M., Ekström, G., Maternovskaya, N.N., 2003. Centroid moment tensor solutions for October–December 2000. Phys. Earth Planet. Inter. 136, 145–164.

Fouch, M.J., Fischer, K.M., 1996. Mantle anisotropy beneath northwest Pacific subduction zones. J. Geophys. Res. 101, 15.987–16.002.

Fouch, M.J., Fischer, K.M., 1998. Shear wave anisotropy in the Mariana subduction zone. Geophys. Res. Lett. 25, 1221–1224.

Frohlich, F., 1989. The nature of deep-focus earthquakes. Ann. Rev. Earth Planet. Sci. 17, 227–254.

Frohlich, C., 1994. Earthquakes with non-double-couple mechanisms. Science 264, 804–809.

Frohlich, C., Davis, S.D., 1999. How well constrained are well-constrained T, B, and P axes in moment tensor catalogs? J. Geophys. Res. 104, 4901–4910.

Fukao, Y., 1984. Evidence from core-reflected shear waves for anisotropy in the Earth's mantle. Nature 309, 695–698.

Gephart, J.W., Forsyth, D.W., 1984. An improved method for determining the regional stress tensor using earthquake focal mechanism data: Application to the San Fernando earthquake sequence. J. Geophys. Res. 89, 9.305–9.320.

Giardini, D., Woodhouse, J.H., 1984. Deep seismicity and modes of deformation in Tonga subduction zone. Nature 307, 505–509.

Giardini, D., 1992. Space-time distribution of deep seismic deformation in Tonga. Phys. Earth Planet. Inter. 74, 75–88.

Gripp, A.E., Gordon, R.G., 1990. Current plate velocities relative to the hotspots incorporating the NUVEL-1 global plate motion model. Geophys. Res. Lett. 17, 1109–1112.

Guest, A., Schubert, G., Gable, C., 2004. Stresses along the metastable wedge of olivine in a subducting slab: Possible explanation for the Tonga double seismic layer. Phys. Earth Planet. Inter. 141, 253–267.

Hamburger, M.W., Isacks, B.L., 1987. Deep earthquakes in the southwest Pacific: a tectonic interpretation. J. Geophys. Res. 92, 13.841–13.854.

Hara, T., Kuge, K., Kawakatsu, H., 1995. Determination of the isotropic component of the 1994 Bolivia deep earthquake. Geophys. Res. Lett. 22, 2265–2268.

Helffrich, G.R., 1997. How good are routinely determined focal mechanisms? Empirical statistics based on a comparison of Harvard, USGS and ERI moment tensors. Geophys. J. Int. 131, 741–750.

Hiramatsu, Y., Ando, M., 1996. Seismic anisotropy near source region in subduction zones around Japan. Phys. Earth Planet. Inter. 95, 237–250.

Hiramatsu, Y., Ando, M., Ishikawa, Y., 1997. ScS wave splitting of deep earthquakes around Japan. Geophys. J. Int. 128, 409–424.

Isacks, B., Molnar, P., 1971. Distribution of stresses in the descending lithosphere from a global survey of focal-mechanism solutions of mantle earthquakes. Rev. Geophys. Space Phys. 9, 103–174.

Julian, B.R., Miller, A.D., Foulger, G.R., 1998. Non-double-couple earthquakes. 1. Theory. Rev. Geophys. 36, 525–549.

Kagan, Y.Y., 2003. Accuracy of modern global earthquake catalogs. Phys. Earth Planet. Inter. 135, 173–209.

Kawakatsu, H., 1991. Insignificant isotropic component in the moment tensor of deep earthquakes. Nature 351, 50–53.

Kawakatsu, H., 1996. Observability of the isotropic component of a moment tensor. Geophys. J. Int. 126, 525–544.

Kawasaki, I., Tanimoto, T., 1981. Radiation patterns of body waves due to the seismic dislocation occurring in an anisotropic source medium. Bull. Seism. Soc. Am. 71, 37–50.

Kendall, J.-M., Thomson, C., 1993. Seismic modelling of subduction zones with inhomogeneity and anisotropy—I. Teleseismic P-wavefront tracking. Geophys. J. Int. 112, 39–66.

Kennett, B.L.N., Engdahl, E.R., Buland, R., 1995. Constraints on seismic velocities in the Earth from travel times. Geophys. J. Int. 122, 108–124.

Kuge, K., Kawakatsu, H., 1992. Deep and intermediate depth non-double couple earthquakes—interpretation of moment tensor inversions using various passbands of very broad-band seismic waves. Geophys. J. Int. 111, 589–606.

Mainprice, D., Barruol, G., Ben Ismail, W., 2000. The seismic anisotropy of the Earth's mantle: from single crystal to polycrystal. In: Karato, S., Forte, A., Liebermann, R.C., Masters, G., Stixrude, L. (Eds.), Earth's Deep Interior, Mineral Physics and Tomography from the Atomic to the Global Scale, Geophysical Monograph Series. American Geophysical Union, Washington, pp. 237–264.

Miller, A.D., Foulger, G.R., Julian, B.R., 1998. Non-double-couple earthquakes 2. Observations. Rev. Geophys. 36, 551–568.

Northard, S., McKenzie, D., Haines, J., Jackson, J., 1996. Gaussian curvature and the relationship between the shape and the deformation of the Tonga slab. Geophys. J. Int. 127, 311–327.

Savage, M.K., 1999. Seismic anisotropy and mantle deformation: What have we learned from shear wave splitting? Rev. Geophys. 37, 65–106.

Šílený, J., Vavryčuk, V., 2000. Approximate retrieval of the point source in anisotropic media: numerical modelling by indirect parametrization of the source. Geophys. J. Int. 143, 700–708.

Šílený, J., Vavryčuk, V., 2002. Can unbiased source be retrieved from anisotropic waveforms by using an isotropic model of the medium? Tectonophysics 356, 125–138.

Sipkin, S.A., Bufe, C.G., Zirbes, M.D., 2000. Moment-tensor solutions estimated using optimal filter theory: global seismicity. Phys. Earth Planet. Inter. 130, 129–142.

Tibi, R., Bock, G., Wiens, D.A., 2003. Source characteristics of large deep earthquakes: constraint on the faulting mechanism at great depths. J. Geophys. Res. 108 (art. No. 2091).

Vavryčuk, V., 2001. Inversion for parameters of tensile earthquakes. J. Geophys. Res. 106 (B8), 16.339–16.355.

Vavryčuk, V., 2004. Inversion for anisotropy from non-double-couple components of moment tensors. J. Geophys. Res. 109, B07306, doi:10.1029/2003JB002926.

Vavryčuk, V., 2005. Focal mechanisms in anisotropic media. Geophys. J. Int. 161, 334–346, doi:10.1111/j.1365-246X.2005.02585.x.

Wookey, J., Kendall, J.-M., Barruol, G., 2002. Mid-mantle deformation inferred from seismic anisotropy. Nature 415, 777–780.

Zhou, H., 1990. Observations on earthquake stress axes and seismic morphology of deep slabs. Geophys. J. Int. 103, 377–401.